Functional Clustering of Systolic Blood Pressure and Frontal Brain Oxygenation During an Active Stand Test in the Irish Longitudinal Study on Aging (TILDA): A Comparison of Tissue Saturation Index Versus Absolute Oxygenated Hemoglobin Concentration Approaches

Feng Xue, Silvin Knight, Emma Connolly, Morgana Afonso Shirsath, Louise Newman, Eoin Duggan, Rose Anne Kenny, and Roman Romero-Ortuno

***Abstract*—Understanding the clinical implications of combined patterns of blood pressure and brain oxygenation dynamics during the transition from lying to standing remains limited. These dynamics can be investigated non-invasively in humans through a standardized active stand (AS) test, which involves continuous monitoring of blood pressure using digital artery photoplethysmography and frontal brain oxygenation using near-infrared spectroscopy (NIRS). While NIRS output is commonly assessed in terms of the tissue saturation index (TSI), it can also be quantified by the absolute concentration of oxygenated hemoglobin (O2Hb). This study aimed to explore functional clustering of systolic blood pressure (sBP) and frontal brain oxygenation during the AS test within the Irish Longitudinal Study on Aging (TILDA), comparing the health correlates of TSI and O2Hb clustered with the K-shape algorithm. A total of 2793 participants from TILDA wave three were included, with a mean age of 64.5 years and 46.9% being male. Both clustering methodologies revealed statistically significant associations with participants' characteristics, including age, sex, body mass index (BMI), pulse wave velocity, cardiovascular medication usage, and usual gait speed. Notably, the TSI_sBP clustering approach uniquely captured variations in the mini-mental state examination (MMSE) cognitive score and history of cardiovascular disease, whereas the O2Hb_sBP clustering method specifically identified variations in poststand orthostatic intolerance (OI) symptoms and future mortality. It was revealed that, when coupled with sBP signal, O2Hb information was associated with a clinically important longitudinal outcome, whereas TSI was not. However, external validation of this finding is warranted to confirm its robustness and generalizability.**

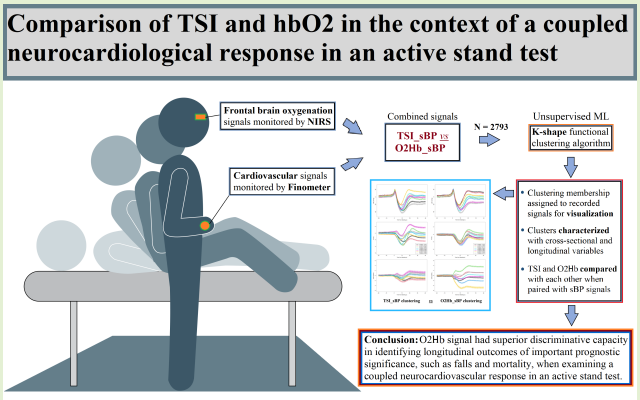

***Index Terms*—Functional clustering, neurocardiovascular signal, oxygenated hemoglobin (O2Hb) concentration, tissue saturation index (TSI).**

Received 28 August 2024; accepted 22 October 2024. Date of publication 5 November 2024; date of current version 2 January 2025. The associate editor coordinating the review of this article and approving it for publication was Dr. Varun Bajaj. *(Corresponding author: Feng Xue.)*

This work involved human subjects or animals in its research. Approval of all ethical and experimental procedures and protocols was granted by the Review Board is Health Sciences Research Ethics Committee of Trinity College Dublin (protocol reference:"Main Wave 3 Tilda Study", approval granted 9 June 2014).

The authors are with the School of Medicine, Trinity College Dublin, Dublin 2, D02 PN40 Ireland (e-mail: fxue@tcd.ie).

Digital Object Identifier 10.1109/JSEN.2024.3488513

I. Introduction

ORTHOSTASIS, the physiological responseto assuming an upright posture plays a pivotal role in regulating blood pressure and ensuring adequate perfusion to vital organs [1], [2]. However, in certain individuals, this mechanism can become dysregulated, leading to orthostatic intolerance (OI) [3]. OI encompasses a spectrum of symptoms, including light-headedness, dizziness, visual disturbance, syncope or near-syncope, palpitations, and fatigue, upon assuming an

upright position [4], [5]. These symptoms often result from inadequate compensatory mechanisms to maintain cerebral perfusion in the upright position [6], [7]. Concurrently, conditions such as vestibular disorder [8] and functional disorder [9] may contribute to the manifestation of OI. The heterogeneous nature of OI symptoms results in adverse health outcomes extending beyond physiological manifestations, adversely impacting daily activities and quality of life [10].

The active stand (AS) test has emerged as a valuable clinical assessment tool for identifying OI by evaluating neurocardiovascular responses to a standard lying-to-standing postural change [11]. Recently, near-infrared spectroscopy (NIRS) has been integrated into the AS to monitor oxygenation indices in the frontal lobe, providing additional insights into cerebral perfusion dynamics [12], [13]. NIRS allows for the continuous noninvasive measurement of oxygenated hemoglobin (O2Hb) and deoxygenated hemoglobin (HHb) concentrations in the cerebral tissue [14], [15]. Oxygenation of the frontal lobe, as assessed by NIRS during an AS test, can serve as an indicator of cerebral oxygen perfusion adequacy as a result of the orthostatic stress [16], [17]. Tissue saturation index (TSI), derived from the ratio of O2Hb to the total hemoglobin concentration (tHb = O2Hb + HHb), is commonly utilized in clinical research settings [18], [19], [20]. It has commonly been used as the representation of the proportion of hemoglobin that is oxygenated within the cerebral tissue, reflecting the balance between oxygen delivery and consumption [21]. While both TSI [22], [23] and O2Hb [24], [25], [26] are routinely used to monitor tissue oxygenation, TSI is often preferred over the measurement of O2Hb alone as it accounts for variations in tHb, arguably offering a more comprehensive assessment of cerebral oxygenation status [27], [28]. However, a study conducted by Mol et al. [29] questioned the reliability of TSI for measuring cerebral oxygenation, possibly due to an insufficient validity of the assumptions needed to compute TSI, such as homogeneity of brain tissue [30], [31].

The implementation of NIRS into the AS test has enabled investigations of the complex interplay between cardiovascular regulation and cerebral perfusion in individuals with OI. However, a comprehensive understanding of these signals remains elusive, including the extent to which the cerebral autoregulation may be able to potentiate the peripheral poststand BP-rising mechanisms, or even replace them when they are impaired; or the extent to which the peripheral BP-rising mechanisms may be sufficient when the cerebral autoregulation is impaired. These physiological scenarios are expected to manifest in diverse combined cardiovascular and cerebrovascular responses, generating distinctive patterns within the intertwined signals. The intricate nature of these signals poses challenges for analysis using conventional methods, considering the complexity of combining two simultaneous recorded time-series data. This is particularly true for large datasets, where uncovering hidden trends and patterns can be challenging, or even not possible without computational aids [32].

Functional clustering, a method derived from unsupervised machine learning, aims to organize functional data into clusters based on their similarity within the functional space [33]. This approach is founded on the premise that functional data, such as time-series, can be modeled and represented by mathematical functions, allowing for comparisons and grouping based on their similarities [34]. Widely utilized across various disciplines including finance, biology, and engineering, functional clustering has found application in medicine for tasks such as identifying disease subtypes [35], exploring gene-disease associations [36], and uncovering diagnostic and prognostic biomarkers [37]. Despite its widespread use, functional clustering remains underutilized in the analysis of noninvasively collected cardiovascular and neurovascular data during the AS test.

This study aimed to explore functional clustering of systolic blood pressure (sBP) and NIRS-measured frontal brain oxygenation during the AS test within the Irish longitudinal study on aging (TILDA), comparing the health correlates of TSI versus O2Hb clustering approaches.

II. Materials and Methods

A. Study Population

The cardiovascular and neurovascular data collected during the AS tests at Wave 3 of TILDA were utilized in this investigation. The third wave of TILDA commenced in 2014 and concluded in 2015. A total of 6687 participants underwent interviews in their own homes, with 80% also undergoing a health assessment, either at their own residence or at a dedicated health assessment center in Trinity College Dublin. The AS test was only conducted at the latter location [38]. Participants under the age of 50 years, and those with missing AS data were excluded from the analysis. The longitudinal outcomes were collected from waves 5 (2018) and 6 (2022). Ethics approval was obtained for each wave from the Faculty of Health Sciences Research Ethics Committee at Trinity College Dublin, Ireland. Written informed consent was provided by all participants, and the research was conducted in adherence to the principles outlined in the Declaration of Helsinki.

B. Active Stand

The AS is a standardized test employed to assess cardiovascular and neurovascular reactions triggered by the action of standing up. Its scope encompasses the evaluation of neurovascular causes associated with OI. During the standardized AS test conducted in TILDA Wave 3 [39], six continuous noninvasive physiological signals were monitored. Within the cardiovascular domain, measurements of the systolic (sBP) and diastolic blood pressure (dBP), as well as heart rate (HR), were captured using a digital artery photoplethysmography device. Simultaneously, within the neurovascular domain, readings of O2Hb, HHb, and TSI of the frontal lobe were recorded via NIRS.

C. Instrumentation

1) Continuous Cardiovascular Signals: A Finometer device (Finometer MIDI, Finapres[1] Medical Systems, Enschede,

[1]Registered trademark.

The Netherlands) was employed to noninvasively measure reconstructed brachial artery pressure on a beat-to-beat (BtB) basis [40]. Operating on photoplethysmography principles, this device captures the pressure waveform from the arteries that run on either side of a finger, at a rate of 200 Hz utilizing the volume-clamp method. The volume of the finger arteries, which is measured by optical sensors embedded in the device, is maintained constant throughout the assessment with the finger cuff actuated by a pneumatic control system [41]. Noteworthy is the robust validation of the volume-clamp method, showing strong agreements with both intra-arterial monitoring [42] and the auscultatory method [43]. Additionally, the Finometer device integrates a position sensor to account for and correct the hydrostatic height of the finger with respect to the heart level.

2) Continuous Neurovascular Signals: NIRS represents a noninvasive and nonionizing technology that has been employed for quantifying fluctuations in oxygenated and deoxygenated hemoglobin concentrations across diverse human tissues [22], [44], [45]. Extensive research shows the coherence of NIRS measurements with other assessment methods in various applications, including cerebral blood flow [46] and skeletal muscle contractions [47]. The versatility and high temporal resolution of NIRS, enabled by its capacity in time-resolved, frequency-domain, and continuous wave spectroscopic implementations, imply its broad potential across an array of applications in both research and clinical settings [48].

Based on optical sensing technology, NIRS measurements capture light absorbance across various wavelengths, where absorbance at approximately 850 nm corresponds to O2Hb and absorbance near 760 nm corresponds to HHb. Frequently, studies report combinations of O2Hb and HHb, such as the TSI, calculated as 100 times O2Hb divided by the sum of O2Hb and HHb ((O2Hb/(O2Hb + HHb)) x 100) [49].

In this study, the PortaLite[1] (Artinis Medical Systems, The Netherlands), a wireless NIRS device, was utilized to measure O2Hb, HHb, and TSI signals employing the absolute concentration method based on spatially resolved spectroscopy. This device features an optical sensor consisting of an emitter and three receivers, enabling transmission of multichannel, real-time data through Bluetooth[1] at a maximum sampling frequency of 50 Hz. Oxysoft v3.0.53 was used as the user interface for the setup, recording, and export of NIRS data. The NIRS sensor was affixed approximately 2 cm above the left eye approximately the FP1 (left frontal) position of the 10–20 electrode system (3 cm lateral and 3.5 cm superior to the nasion) [50], with a consistent sampling frequency of 50 Hz applied across all participants. To mitigate the influence of ambient light, a blackout headband was used to cover the sensor [39].

D. Signal Acquisition, Synchronization, and Preprocessing

A one-minute segment of the AS data, spanning from 20 s before standing to 40 s after, was the focus of this study. The BtB cardiovascular signals from the Finapres[1] MIDI were interpolated at a rate of 5 Hz, while the neurovascular signals recorded by NIRS were downsampled to match this frequency. The Finapres[1] device provides sBP measures in a BtB format, whereas the NIRS device measures data continuously at 50 Hz. Due to this discrepancy in sampling methods, and to allow comparability between data, BtB data were interpolated to 5 Hz, and NIRS data were decimated to 5 Hz. The 5 Hz sampling frequency was chosen as it captures shape changes while minimizing nonphysiological noise. This approach is also consistent with the convention used in previous TILDA NIRS/sBP studies [39], [51]. To ensure synchronization, all signals were aligned using multiple manual markers placed throughout the recordings. The onset of the stand (i.e., the moment participants started standing up from the supine position) was detected using an algorithm previously described in detail by O'Connor et al. [52], based on the Finapres[1] MIDI's height sensor data. Baseline values for the cardiovascular and neurovascular signals were computed by averaging readings from 60 to 30 s prior to standing (in supine resting position), in keeping with previous investigations [11], [39], [53].

Regarding data cleaning steps, the data used in this study were unfiltered initially, as this aligned with the study's purpose. However, several data cleaning procedures were routinely applied to the Finapres[1] data after collection. These included filtering out data with abnormal height sensor readings, undetected beats, and considering notes written by the research nurses during data collection. Additionally, the exclusion criteria for NIRS data were as follows.

1) Implausible mean TSI.
2) *TSI Too Low:* too many values < 10 ("too many values" was defined as more than 4 of the values in the AS signal).
3) *O2Hb Too Low:* too many values < 0.1.
4) *HHb Too Low:* too many values < 0.1.
5) *Flat TSI Signal:* the data team checked if the absolute difference between consecutive values was $<= 1e^{-05}$ in over a quarter of the recordings.

In addition to the above routine quality checks, one obvious outlier was visually identified in the sBP plot and removed from the analysis.

Plots of unprocessed signals, separately for sBP, TSI, and O2Hb, are shown in Fig. 1. To balance the magnitude of shape change within the region of interest among the signals, these time-series were normalized against the standard deviation of the baseline recordings. To prepare for K-shape clustering analysis of paired neurovascular-cardiovascular signals, TSI and O2Hb signals were adjoint with sBP separately, yielding two coupled signals, TSI_sBP (Fig. 2) and O2Hb_sBP (Fig. 3), respectively. To ensure a smooth connection between the two adjoining signals, the normalized TSI and O2Hb time-series were reversed before adjoining the sBP signal, which greatly reduced the difference in magnitude at the junction between each pair of signals, keeping the introduction of shape information minimal during preprocessing.

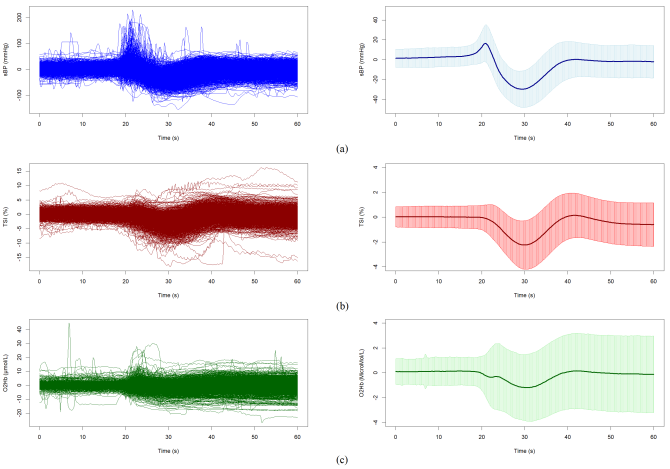

Fig. 1. Raw data of (a) sBP, (b) TSI, and (c) O2Hb signals with corresponding mean ± SD plots shown on the right. Baseline values had been deducted from each signal for each participant, resulting in the relative changes shown in the plots.

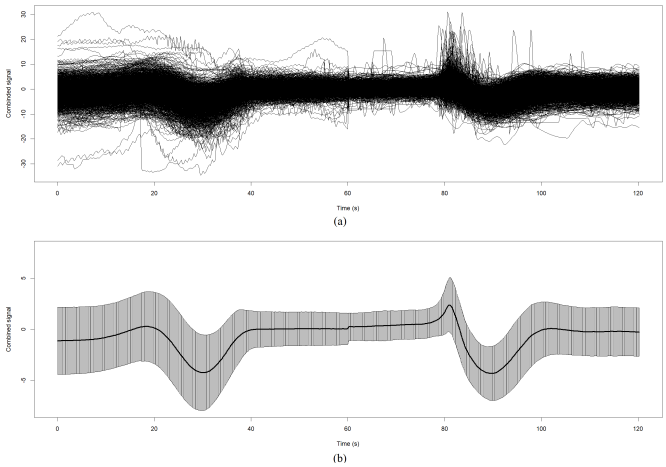

Fig. 2. (a) Combined signals of TSI and sBP, with (b) corresponding mean ± SD plots shown in joint at which the two signals were combined is shown at 60 s.

E. Functional Clustering

We employed the K-shape functional clustering algorithm, developed by Paparrizos and Gravano [54] in 2015. Similar to K-means, K-shape initializes a predetermined number of clusters and then assigns each time-series to its corresponding cluster based on distances calculated to the updated centroid locations through iterative processes. However, unlike K-means, which groups data points relying on positional information within the Euclidean space, K-shape employs shape-based distance (SBD) as defined as follows:

$$\mathrm{SBD}(\vec{x}, \vec{c_k}) = 1 - \max_{\omega} \left(\frac{CC_{\omega}(\vec{x}, \quad \vec{c_k})}{\sqrt{\mathrm{R}_0(\vec{x}, \quad \vec{x}) \cdot \mathrm{R}_0(\vec{c_k}, \vec{c_k})}} \right) \tag{1}$$

where ω is the position at which the cross correlation $CC_{\omega}(\vec{x}, \vec{c_k})$ between each z-normalized sequence $\vec{x}$, and the centroid vector of each cluster $\vec{c_k}$ was maximized; R_0 is the geometric mean of autocorrelation of each individual sequence $\vec{x}$ or $\vec{c_k}$. Cross correlation measures the degree of similarity

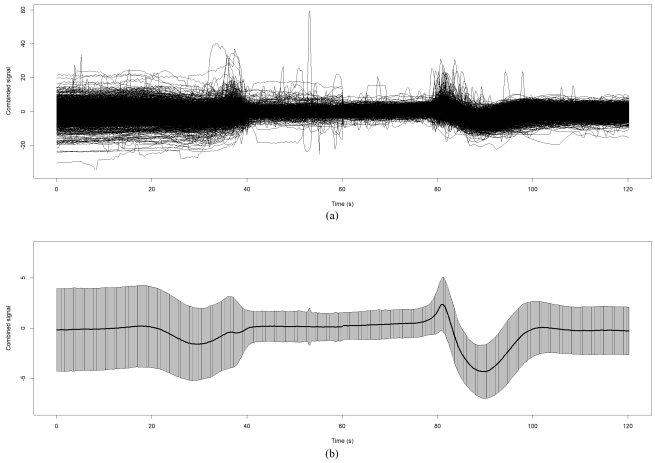

Fig. 3. (a) Combined signals of O2Hb and sBP, with (b) corresponding mean ± SD plots shown in (b) joint at which the two signals were combined is shown at 60 s.

between two sequences, in this case two time series, calculated as a function of the displacement of $\vec{x}$ over the centroid of the cluster it belongs to, $\vec{c_k}$.

The K-shape clustering algorithm was implemented in the *dtwclust* package (version 5.5.11) in R version 4.0.5 using RStudio 2022.07.1 + 554 (Boston, MA, USA). The joined TSI_sBP and O2Hb_sBP data were entered into the K-shape algorithm, with type = "partitional," distance = "sbd," centroid = "shape" and the number of clusters set at eight based on gap statistic measures for the data.

Gap statistic is a method for determining the optimal number of clusters in a dataset using unsupervised learning. The basic idea behind the gap statistic is to compare the within-cluster variation of a clustering solution against that expected under an appropriate reference null distribution [55]. It is expressed as

$$\mathrm{Gap}_n(k) = E_n^*\{\log(W_k)\} - \log(W_k) \tag{2}$$

where k is the number of clusters and $E[\log(W_k)]$ is the expected value of the log of within-cluster variation of the reference dataset under the null distribution. The gap statistic serves as a robust method for determining the ideal number of clusters, exhibiting resilience against initial conditions due to its iterative execution on the provided data via bootstrap resampling. This approach ensures stability and reliability in estimating the optimal clustering configuration. The R package *factoextra* (version 1.0.7) was used to compute the gap statistic. The optimal number of clusters was determined using the "firstSEmax" method, which identifies the smallest k such that its value $f(k)$ is not more than 1 standard error away from the first local maximum. This method was the default setting in *factoextra*. We set the maximum number of clusters at eight based on insights from a previous pilot study [56], taking into account that exceeding eight clusters could diminish both the clinical interpretability of the results and the statistical power for the between-cluster comparisons. With a bootstrap of 100, 8 was indicated as the optimum number of clusters for both datasets, shown as the broken

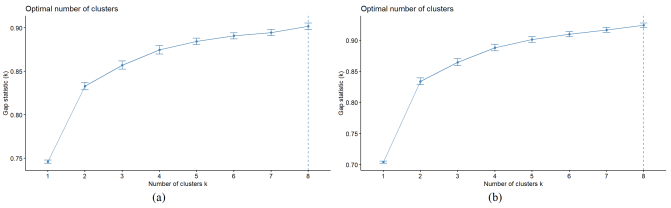

Fig. 4. Gap statistic plots for the coupled (a) TSI_sBP and (b) O2Hb_sBP signals.

vertical lines in Fig. 4(a) and (b), for TSI_sBP and O2Hb_sBP clustering setup, respectively.

F. Statistical Analyses

The statistical analyses for cluster characterization were conducted using R version 4.0.5. Overall comparisons among the clusters involved the independent-samples Kruskal–Wallis test for nonnormally distributed continuous variables, and the Chi-square test for categorical variables. Post-hoc pairwise comparisons were conducted with Bonferroni correction. The threshold for statistical significance was set at $P < 0.05$.

G. Characterization Variables

For cluster characterization, we employed both cross-sectional (wave 3) variables and longitudinal outcomes from future TILDA waves. The summary of these variables is provided below:

Cross-sectional variables.

1) Mean age in years.
2) Percentage of male participants.
3) Mean body mass index (BMI) in kg/m^2.
4) Percentage of participants with self-reported cardiovascular disease (0: no; 1: yes).
5) Percentage of participants with heart disease (0: no; 1: yes).
6) Percentage of participants with cerebrovascular disease (stroke or TIA/ministroke: 0: no; 1: yes).
7) Percentage of participants with diabetes mellitus (0: no; 1: yes).
8) Percentage of participants taking cardiovascular medications (0: no; 1: Yes).
9) Percentage of participants taking psychotropic medications (0: no; 1: Yes).
10) Mean pulse wave velocity in m/s (pulse wave velocity measurement between the carotid and femoral arteries—a noninvasive method of measuring arterial stiffness) [57].
11) Mean minimental state examination (MMSE) cognitive score.
12) Mean usual gait speed in cm/s.
13) Percentage of participants with self-reported falls in the past year (0: no; 1: yes).
14) Percentage of participants reporting OI post-AS (0: no; 1: yes)

Longitudinal variables.

1) Percentage of participants experiencing any fall by wave 6 (0: no; 1: yes).

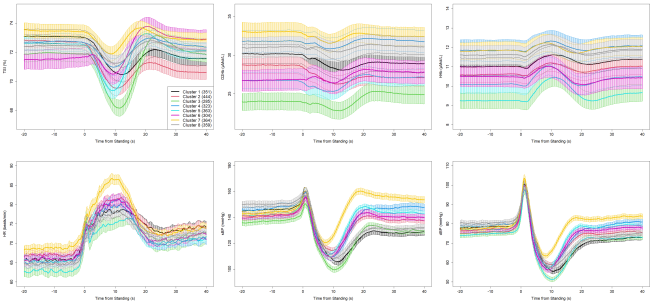

Fig. 5. Visualization of the eight clusters (based on coupled TSI_sBP signals) for all six original raw signals, including cerebrovascular signals (upper row): TSI, O2Hb, and HHb; and cardiovascular signals (lower row): HR, sBP, and dBP. For each signal, the mean is shown as the solid line, and the 95% confidence interval is the surrounding shaded area. Recovery period refers to the time after standing took place at 0 s in each plot. Note that the TSI and sBP were the host signals in this clustering setup, based on which the clustering membership was assigned to all six signals.

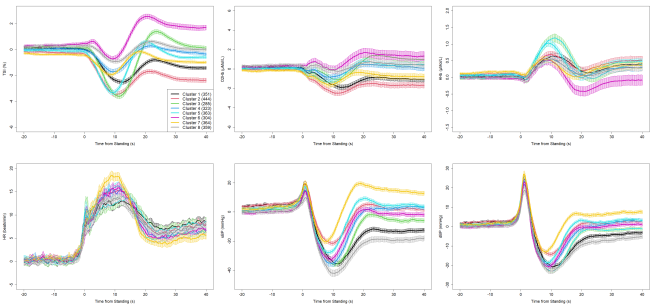

Fig. 6. Visualization of the eight clusters (based on coupled TSI_sBP signals) for all six signals (with baseline values deducted from each original raw signal), including cerebrovascular signals (upper row): TSI, O2Hb, and HHb; and cardiovascular signals (lower row): HR, sBP, and dBP. For each signal, the mean is shown as the solid line and the 95% confidence interval is the surrounding shaded area. Recovery period refers to the time after standing took place at 0 s in each plot. Note that the TSI and sBP were the host signals in this clustering setup, based on which the clustering membership was assigned to all six signals.

2) Percentage of participants deceased by wave 6 (0: no; 1: yes).

III. Results

The cohort for this study comprised a total of 2793 participants, with 46.9% being male. The mean age of the entire cohort was 64.5 years. Regarding the clustering analysis, gap statistic plots for the merged TSI_sBP and O2Hb_sBP signals indicated that the optimal number of clusters was 8, as denoted by the dotted line, for both clustering setups (Fig. 4).

The graphical overview of the eight clusters is shown in Figs. 5 and 6, for the TSI_sBP clustering setup, and Figs. 7 and 8 for the O2Hb_sBP clustering setup, respectively. Both neurovascular signals (TSI, O2Hb, HHb) and cardiovascular signals (sBP, dBP, HR) were plotted in each figure.

The results of cluster characterization are shown in Tables I and II, for TSI_sBP and O2Hb_sBP, respectively. Due to the nature of random seeding [58] used in the algorithm for implementing the K-shape clustering, the cluster numbers do not correspond between the two clustering setups and should be considered separately when interpreting the

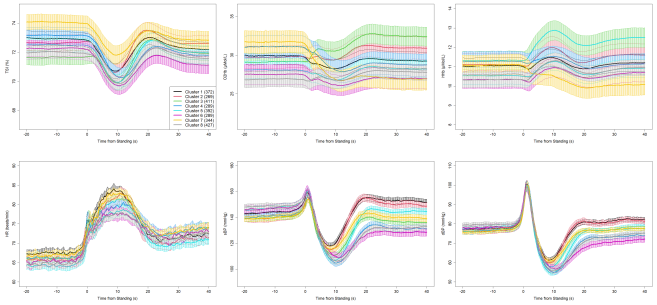

Fig. 7. Visualization of the eight clusters (based on coupled O2Hb_sBP signals) for all six original raw signals, including cerebrovascular signals (upper row): TSI, O2Hb, and HHb; and cardiovascular signals (lower row): HR, sBP, and dBP. For each signal, the mean is shown as the solid line and the 95% confidence interval is the surrounding shaded area. Recovery period refers to the time after standing took place at 0 s in each plot. Note that the O2Hb and sBP were the host signals in this clustering setup, based on which the clustering membership was assigned to all six signals.

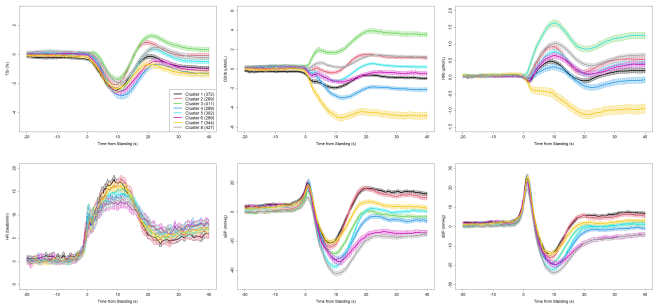

Fig. 8. Visualization of the eight clusters (based on coupled O2Hb_sBP signals) for all six signals (with baseline values deducted from each original raw signal), including cerebrovascular signals (upper row): TSI, O2Hb, and HHb; and cardiovascular signals (lower row): HR, sBP, and dBP. For each signal, the mean is shown as the solid line, and the 95% confidence interval is the surrounding shaded area. Recovery period refers to the time after standing took place at 0 s in each plot. Note that the O2Hb and sBP were the host signals in this clustering setup, based on which the clustering membership was assigned to all six signals.

results. Both clustering methodologies revealed statistically significant associations with participants' characteristics, including age, sex, BMI, pulse wave velocity, cardiovascular medication usage, and usual gait speed. Notably, the TSI_sBP clustering approach uniquely captured variations in the MMSE cognitive score and history of cardiovascular disease, whereas the O2Hb_sBP clustering method specifically identified variations in post-stand OI symptoms and future mortality.

IV. Discussion

In this study, we performed K-shape functional clustering of noninvasively collected, continuous cardiovascular and neurovascular signals during an AS test in a large population-based sample. Our aim was to compare the clinical relevance of TSI, a commonly used derived variable, with that of O2Hb, a directly measured variable for brain oxygenation, in the context of the combined shape signatures of neurocardiovascular response. Eight clusters were obtained for both clustering setups and characterized separately with both cross-sectional and longitudinal variables in TILDA. While both approaches captured significant differences between the clusters, it was revealed that, when coupled with sBP signal, O2Hb information was associated with clinically important associations such as OI and mortality, whereas TSI was not.

From a cross-sectional characterization perspective, the TSI_sBP clustering approach uniquely captured variations in MMSE score and history of cardiovascular disease. Cluster 2 had the second-highest proportion of cardiovascular disease (64.4%), while cluster 3 had the lowest proportion (51.9%). Similarly, for MMSE scores, cluster 2 shared the highest mean score (29.1 points), and cluster 3 had the lowest score (28.8), although these small differences (<1 point) in mean MMSE are unlikely to be clinically significant [59]. Looking at the neurovascular profiles, the unhealthier-looking cluster 2 (red lines, $N = 444$) was characterized by the largest absolute (Fig. 5) and relative (Fig. 6) TSI drops by 40 s post-stand and the most pronounced O2Hb drop relative to baseline (Fig. 6). On the other hand, the healthier cluster 3 (green lines, $N = 285$) exhibited a vigorous TSI overshoot between 10 and 20 s poststand, with average sBP and dBP recoveries by 40 s poststand.

As regards poststand OI and future mortality, only the O2Hb_sBP clustering approach revealed significant differences between clusters. Pairwise analyses suggested that cluster 6 was unhealthier with the highest OI proportion (38.3%); additionally, it had the second highest mortality proportion (7.3%), contrasting with cluster 1 which had the second lowest OI proportion (24.6%) and the lowest mortality (1.9%). Looking at their neurovascular profiles in Fig. 7, cluster 6 (pink lines, $N = 289$) had the lowest absolute TSI and BP values poststand. In contrast, cluster 1 (black lines, $N = 372$), displayed the most vigorous BP responses by 40 s post-stand, as seen in Figs. 7 and 8.

Visual inspection of Figs. 5–8 suggested that clustering by TSI seemed to result in capturing mainly overall mean magnitude differences in O2Hb and HHb signals (Fig. 5), resulting in this approach capturing less information with regards complex shape change of these signals from baseline (Figs. 6 versus 8). This most likely derives from the fact that TSI is a composite of O2Hb and HHb measures. Conversely, clustering by O2Hb appeared to capture more complex patterns of relative shape changes in O2Hb and HHb, as shown in Fig. 8. This may be a factor contributing to the greater performance of this approach with regards associations with OI and mortality.

Our results are in keeping with previous observations by Fitzgibbon-Collins et al. [60] who explored the link between posture-related reductions in cerebral tissue oxygenation and postural stability in older adults, finding that lower oxygenation during standing was associated with increased instability and potentially higher fall risk. Even though in our O2Hb_sBP clustering the overall significant difference in future falls ($P = 0.022$) did not achieve significance in the Bonferroni-adjusted pairwise comparisons, overall difference in future falls was not detected by the TSI_sBP clustering approach. Moreover, a study by Klop et al. [61] compared NIRS-measured oxygenation with continuous BP and cerebral blood velocity (CBv) in 41 participants, finding

TABLE I
TSI_sBP CLUSTER CHARACTERISTICS

	Cluster 1 (n=351)	Cluster 2 (n=444)	Cluster 3 (n=285)	Cluster 4 (n=323)	Cluster 5 (n=363)	Cluster 6 (n=304)	Cluster 7 (n=364)	Cluster 8 (n=359)	Overall p value and significant pairwise comparisons (cluster number)
Mean baseline SBP (mmHg)	144.1	139	142.9	141.8	136.2	140.8	148.4	150.3	<0.001 (1-2, 1-3, 1-8, 2-4, 2-6, 2-7, 2-8, 3-4, 3-6, 3-7, 3-8, 4-5, 4-8, 5-8, 6-8, 7-8)
Mean baseline DBP (mmHg)	76.7	75.7	76.2	77	74.6	76.4	79.4	80.5	<0.001 (1-2, 1-8,2-4, 2-5, 2-6, 2-7, 2-8, 3-4, 3-6, 3-7, 3-8, 5-8, 6-8, 7-8)
Mean baseline HR (bpm)	64	65.1	65	65.5	66.7	68.2	64.5	64.6	<0.001 (1-3, 1-7, 2-3, 3-6, 3-7, 4-7, 5-7, 6-7, 7-8)
Mean baseline TSI (%)	72.5	72.7	72.2	71.2	74.2	73.8	71.8	72.2	<0.001 (1-3, 1-6, 2-3, 2-6, 3-7, 4-6, 5-6, 5-7, 6-7, 7-8)
Mean baseline O2Hb (µmol/L)	28	26.7	27.4	26.5	31.7	33.2	26.6	30.7	<0.001 (1-3, 1-5, 1-6, 1-7, 2-3, 2-4, 2-7, 3-4, 3-5, 3-7, 3-8, 4-5, 4-6, 5-7, 5-8, 6-7, 6-8, 7-8)
Mean baseline HHb (µmol/L)	10.5	10	10.3	10.5	11	11.7	10.3	11.6	<0.001 (1-3, 2-3, 2-4, 2-7, 2-8, 3-4, 3-6, 3-7, 3-8, 4-5, 5-7, 5-8, 6-7)
Mean age, years	64.1	63.7	67.4	63.3	64.4	62.3	65.9	65.5	<0.001 (1-4, 1-5, 1-6, 1-7, 2-7, 3-5, 3-6, 3-7, 4-7, 5-8, 6-8, 7-8)
Male sex (%)	44.2	48.2	75.4	32.5	57	57.6	31.9	34	<0.001 (1-3, 1-5, 1-6, 1-7, 2-3, 2-4, 2-7, 2-8, 3-4, 3-5, 3-6, 3-7, 3-8, 4-5, 4-6, 5-7, 5-8, 6-7, 6-8)
Mean BMI (kg/m^2)	28.5	28.5	27.5	28.2	29.1	30	27.2	27.1	<0.001 (1-7, 2-7, 3-4, 3-5, 3-84-6, 4-7, 5-7, 6-8, 7-8)
Cardiovascular disease (%)	65	64.4	51.9	62.5	56.7	54.6	59.1	63.2	0.002 (1-3, 2-3)
Heart disease (%)	5.4	4.7	6.3	3.4	2.2	2	3	3.3	0.039*
Cerebrovascular disease (%)	2.6	0.9	0.7	0	0.8	1.6	1.4	0.8	0.084
Diabetes (%)	7.4	9.7	6.7	5.3	5.8	5.9	4.7	5.6	0.110
Cardiovascular medication (%)	48.4	43.5	36.8	34.7	32.2	27.3	30.5	42.9	<0.001 (1-4, 1-5, 1-6, 1-7, 2-5, 2-6, 2-7, 3-8, 6-8, 7-8)
Psychotropic medication (%)	14.8	10.6	12.6	13.6	11.6	13.5	11.3	13.1	0.690
Mean pulse wave velocity (m/s)	10.5	10.2	10.9	10.1	10.2	10.3	10.6	10.6	<0.001 (1-5, 1-6, 5-8, 6-8)
Mean MMSE score	29.1	29.1	28.8	29.1	28.9	29.1	28.9	28.9	0.003 (2-7, 7-8)
Mean usual gait speed (cm/s)	138.8	140.1	131.7	142.3	135.8	137.6	136	135.4	<0.001 (1-3, 1-5, 1-6, 2-5, 2-6, 4-6, 5-8, 6-8)
Falls history (%)	23.9	24.6	19.6	24.1	17.9	20.1	20.3	22	0.249
Post-AS dizziness (%)	29.2	30.6	34.9	29.7	24.8	29.9	26.4	32.1	0.140
Any fall by wave 6 (%)	52.7	53.2	47.4	50.2	44.4	44.7	47.8	52.6	0.077
Deceased by wave 6 (%)	6.6	6.8	8.4	4.6	3.9	3.9	3.3	6.1	0.046*

Continuous variables were compared across clusters with the Independent-Samples Kruskal-Wallis Test; dichotomous variables with the Chi-square test; * Bonferroni-adjusted pairwise comparisons did not reach statistical significance.

good early correlations between BP and oxygenation, but weaker associations between CBv and oxygenation, suggesting that NIRS may effectively reflect cerebral blood flow during the initial stages of postural transitions in OH.

Methodologically, we believe that the implementation of K-shape functional clustering algorithm on the adjoint neurocardiovascular signals was appropriate, based on the fact that, despite the algorithm being primarily applied to time series data, the distance measure used in the algorithm, SBD, is not inherently temporal-dependent [54]. Thanks to the signal preprocessing procedures used in this study, which resulted in smooth connections at the joints between neurovascular and cardiovascular signals, a minimal introduction of undesired shape information in the combined signals was achieved. This ensured that the K-shape algorithm captured the features intrinsic to the original signals to the maximum extent, maximizing the accuracy of clustering results.

TABLE II
O2Hb_sBP Cluster Characteristics

	Cluster 1 (n=372)	Cluster 2 (n=269)	Cluster 3 (n=411)	Cluster 4 (n=289)	Cluster 5 (n=392)	Cluster 6 (n=289)	Cluster 7 (n=344)	Cluster 8 (n=427)	Overall p value and significant pairwise comparisons (cluster number)
Mean baseline SBP (mmHg)	139.1	141.2	138.8	135.8	139.4	135.5	137.1	144.6	<0.001 (1-8, 2-8, 3-8, 4-5, 4-8, 5-7, 6-7, 6-8, 7-8)
Mean baseline DBP (mmHg)	75.3	76.2	75.8	73.2	76.4	74.2	74.7	77.7	<0.001 (1-8, 2-8, 3-8, 4-8, 6-8, 7-8)
Mean baseline HR (bpm)	66.5	65.7	65.4	66.3	65.9	62.8	65.9	64.6	0.001 (1-5, 5-7, 7-8)
Mean baseline TSI (%)	73.1	73	72.7	73	71.6	71.8	73.1	72.7	<0.001 (1-3, 1-8, 2-7, 3-4, 3-7, 4-8, 5-7, 6-7, 7-8)
Mean baseline O2Hb (µmol/L)	30.2	29.9	29.7	28.8	28.8	23.9	30.8	31.7	<0.001 (1-6, 1-8, 2-8, 4-6, 4-8, 5-7, 6-7, 7-8)
Mean baseline HHb (µmol/L)	11	11	11.1	10.5	11.3	9.3	11.2	11.8	0.025*
Mean age (years)	63.2	66.3	62.6	64.8	63.4	66.1	65.1	64.2	<0.001 (1-4, 1-6, 1-8, 2-4, 2-6, 2-8, 3-6, 3-8, 4-6, 5-6, 6-7)
Male sex (%)	40.1	48	55	50.2	46.7	46.7	46.5	42.6	0.002 (1-3, 3-8)
Mean BMI (kg/m^2)	29.5	27.9	29.2	28.6	27.6	27.5	28.6	28.7	<0.001 (1-3, 1-6, 1-8, 2-3, 2-6, 2-8, 3-7, 4-8, 5-6, 5-8, 6-7, 7-8)
Cardiovascular disease (%)	56.2	61.3	57.9	66.1	59.7	60.2	60.8	60.4	0.350
Heart disease (%)	4.3	4.1	1	5.2	5.1	4.8	2.9	3.7	0.046*
Cerebrovascular disease (%)	0.5	0.7	1.2	1	0.3	2.1	1.5	1.6	0.331
Diabetes (%)	7.3	3.7	5.4	7.3	6.1	8.3	6.7	7	0.448
Cardiovascular medication (%)	33.3	34.9	31.1	41.5	33.7	46.4	37.2	43.3	<0.001 (1-6, 3-6, 3-8, 5-6)
Psychotropic medication (%)	12.1	6.7	10.7	12.1	15.8	15.2	11.9	14.3	0.019*
Mean pulse wave velocity (m/s)	10.6	10.8	10.1	10.3	10.2	10.7	10.5	10.6	<0.001 (2-6, 2-8, 3-6, 5-6, 6-7)
Mean MMSE score	28.9	28.9	29.2	28.8	29.1	28.9	29	29	0.051
Mean usual gait speed (cm/s)	139	134.1	140.2	135.5	140.6	140	136.9	136.6	<0.001 (1-6, 2-6, 3-6, 3-7, 3-8, 5-6)
Falls history (%)	21.8	16.4	17	23.5	23	23.9	24.1	23.7	0.057
Post-AS dizziness (%)	24.6	24.2	31.9	29.5	28.1	38.3	28.3	31.5	0.003 (1-6, 2-6)
Any fall by wave 6 (%)	48.7	42	44	54.3	50	51.6	52.9	51.3	0.022*
Deceased by wave 6 (%)	1.9	4.8	3.9	7.3	5.6	7.3	5.8	7.5	0.009 (1-4, 1-6, 1-8)

Continuous variables were compared across clusters with the Independent-Samples Kruskal-Wallis Test; dichotomous variables with the Chi-square test.; * Bonferroni-adjusted pairwise comparisons did not reach statistical significance.

From a technical perspective, we demonstrated that plotting all six continuous physiological signals in a synchronized fashion, as shown in Figs. 5–8, provided not only an efficient way to visually inspect the physiological responses of different groups during the AS but also made it possible to postulate possible connections between cardiovascular and neurovascular responses, allowing for the generation of hypotheses to be tested in further studies. The addition of functional clustering results in the plots enriches the availability of the stratified information embedded in the assessment data, making it possible in the future to provide a machine learning based knowledge pool for the early detection of deteriorating health. Indeed, it may be possible to identify individual risk based on similarity to a cluster, and this approach can be applied in future clinical research outside population-based studies.

To our knowledge, our study is the first to investigate the clinical relevance of TSI versus O2Hb coupled with cardiovascular data in the context of an orthostatic challenge using an unsupervised machine learning approach. A strength of the current study is the data-driven nature of the methodology, which eliminates subjective influences on the clustering outcome. Another strength is that the study is based on a large population-based sample from which the

physiological data were collected. However, despite the large departing sample size, the sizes of the resulting clusters were relatively modest, precluding subanalysis by sex, which could be of potential interest [62]. Another limitation was that some variables used in this study (including OI) were self-reported. However, mortality is a reliable outcome in TILDA [63]. We also acknowledge that while TILDA offers insights into the Irish community-dwelling context, it will be important to replicate the research in different settings to enhance the external validity of our findings. Our study was not intended to maximize the prediction of clinical outcomes such as OI, falls or mortality risk, but instead emphasizes the importance of considering both signals simultaneously, which could facilitate further comparative clinical research in the future, beyond this research-oriented, population-based setting.

V. Conclusion

Our findings in TILDA suggested that, compared to TSI, the O2Hb signal recorded by NIRS had superior discriminative capacity in identifying associations of important clinical and prognostic significance, such as OI and mortality, when examining a coupled neurocardiovascular response in an AS test. However, external validation of this finding is warranted to confirm its robustness and generalizability.

Acknowledgment

The authors greatly appreciate the opportunity provided by TILDA for granting access to their data and would like to acknowledge the continued commitment and cooperation of the TILDA participants and research team.

References

[1] M. P. M. Harms, W. N. J. M. Colier, W. Wieling, J. W. M. Lenders, N. H. Secher, and J. J. van Lieshout, "Orthostatic tolerance, cerebral oxygenation, and blood velocity in humans with sympathetic failure," *Stroke*, vol. 31, no. 7, pp. 1608–1614, Jul. 2000.

[2] Y.-C. Tzeng and P. N. Ainslie, "Blood pressure regulation IX: Cerebral autoregulation under blood pressure challenges," *Eur. J. Appl. Physiol.*, vol. 114, no. 3, pp. 545–559, Mar. 2014.

[3] J. M. Stewart, "Common syndromes of orthostatic intolerance," *Pediatrics*, vol. 131, no. 5, pp. 968–980, May 2013.

[4] R. Freeman et al., "Consensus statement on the definition of orthostatic hypotension, neurally mediated syncope and the postural tachycardia syndrome," *Autonomic Neurosci.*, vol. 161, nos. 1–2, pp. 46–48, Apr. 2011.

[5] R. Garner and J. N. Baraniuk, "Orthostatic intolerance in chronic fatigue syndrome," *J. Transl. Med.*, vol. 17, no. 1, p. 185, 2019.

[6] J. M. Stewart, "Mechanisms of sympathetic regulation in orthostatic intolerance," *J. Appl. Physiol.*, vol. 113, no. 10, pp. 1659–1668, Nov. 2012.

[7] N. C. S. Lewis et al., "Impact of hypocapnia and cerebral perfusion on orthostatic tolerance," *J. Physiol.*, vol. 592, no. 23, pp. 5203–5219, Dec. 2014.

[8] C. Best, "Interaction of somatoform and vestibular disorders," *J. Neurol., Neurosurg. Psychiatry*, vol. 77, no. 5, pp. 658–664, May 2006.

[9] I. Nozawa, S.-I. Imamura, K. Hashimoto, and Y. Murakami, "Psychosomatic aspects of patients complaining of dizziness or vertigo with orthostatic dysregulation," *Auris Nasus Larynx*, vol. 25, no. 1, pp. 33–38, Jan. 1998.

[10] B. C. D. Hockin, N. D. Heeney, D. G. T. Whitehurst, and V. E. Claydon, "Evaluating the impact of orthostatic syncope and presyncope on quality of life: A systematic review and meta-analysis," *Frontiers Cardiovascular Med.*, vol. 9, Feb. 2022, Art. no. 834879.

[11] C. Finucane et al., "A practical guide to active stand testing and analysis using continuous beat-to-beat non-invasive blood pressure monitoring," *Clin. Autonomic Res.*, vol. 29, no. 4, pp. 427–441, Aug. 2019.

[12] N. Lehmann et al., "Brain activation during active balancing and its behavioral relevance in younger and older adults: A functional near-infrared spectroscopy (fNIRS) study," *Frontiers Aging Neurosci.*, vol. 14, Mar. 2022, Art. no. 828474.

[13] A. Mol, J. A. H. R. Claassen, A. B. Maier, R. J. A. van Wezel, and C. G. M. Meskers, "Determinants of orthostatic cerebral oxygenation assessed using near-infrared spectroscopy," *Autonomic Neurosci.*, vol. 238, Mar. 2022, Art. no. 102942.

[14] G. Strangman et al., "A quantitative comparison of simultaneous BOLD fMRI and NIRS recordings during functional brain activation," *NeuroImage*, vol. 17, no. 2, pp. 719–731, Oct. 2002.

[15] M. Ferrari, L. Mottola, and V. Quaresima, "Principles, techniques, and limitations of near infrared spectroscopy," *Can. J. Appl. Physiol.*, vol. 29, no. 4, pp. 463–487, Aug. 2004.

[16] R. Aaslid, K. F. Lindegaard, W. Sorteberg, and H. Nornes, "Cerebral autoregulation dynamics in humans," *Stroke*, vol. 20, no. 1, pp. 45–52, Jan. 1989.

[17] V. Novak, J. M. Spies, P. Novak, B. R. McPhee, T. A. Rummans, and P. A. Low, "Hypocapnia and cerebral hypoperfusion in orthostatic intolerance," *Stroke*, vol. 29, no. 9, pp. 1876–1881, Sep. 1998.

[18] I. Tachtsidis et al., "Relationship between brain tissue haemodynamics, oxygenation and metabolism in the healthy human adult brain during hyperoxia and hypercapnea," *Adv. Exp. Med. Biol.*, vol. 645, pp. 315–320, 2009.

[19] D. Highton, C. Elwell, and M. Smith, "Noninvasive cerebral oximetry: Is there light at the end of the tunnel?" *Current Opinion Anaesthesiol.*, vol. 23, no. 5, pp. 576–581, 2010.

[20] A. Monaghan, G. Jennings, F. Xue, L. Byrne, E. Duggan, and R. Romero-Ortuno, "Orthostatic intolerance in adults reporting long COVID symptoms was not associated with postural orthostatic tachycardia syndrome," *Frontiers Physiol.*, vol. 13, Mar. 2022, Art. no. 833650.

[21] B. W. Pogue and M. S. Patterson, "Review of tissue simulating phantoms for optical spectroscopy, imaging and dosimetry," *J. Biomed. Opt.*, vol. 11, no. 4, 2006, Art. no. 041102.

[22] M. Ferrari and V. Quaresima, "A brief review on the history of human functional near-infrared spectroscopy (fNIRS) development and fields of application," *NeuroImage*, vol. 63, no. 2, pp. 921–935, Nov. 2012.

[23] K. J. Smith and P. N. Ainslie, "Regulation of cerebral blood flow and metabolism during exercise," *Exp. Physiol.*, vol. 102, no. 11, pp. 1356–1371, Nov. 2017.

[24] T. J. Huppert, S. G. Diamond, M. A. Franceschini, and D. A. Boas, "HomER: A review of time-series analysis methods for near-infrared spectroscopy of the brain," *Appl. Opt.*, vol. 48, no. 10, pp. 280–298, 2009.

[25] K. L. M. Koenraadt, E. G. J. Roelofsen, J. Duysens, and N. L. W. Keijsers, "Cortical control of normal gait and precision stepping: An fNIRS study," *NeuroImage*, vol. 85, pp. 415–422, Jan. 2014.

[26] Y. Ishii et al., "The changes in concentration of cerebral oxygenated hemoglobin during single event-related Japanese shiritori task in patients with major depression disorder: Comparison with healthy subjects," *Frontiers Psychiatry*, vol. 12, Oct. 2021, Art. no. 709771.

[27] T. Durduran et al., "Diffuse optical measurement of blood flow, blood oxygenation, and metabolism in a human brain during sensorimotor cortex activation," *Opt. Lett.*, vol. 29, no. 15, pp. 1766–1768, 2004.

[28] M. M. Tisdall, I. Tachtsidis, T. S. Leung, C. E. Elwell, and M. Smith, "Near-infrared spectroscopic quantification of changes in the concentration of oxidized cytochrome C oxidase in the healthy human brain during hypoxemia," *J. Biomed. Opt.*, vol. 12, no. 2, 2007, Art. no. 024002.

[29] A. Mol, J. H. H. Woltering, W. N. J. M. Colier, A. B. Maier, C. G. M. Meskers, and R. J. A. van Wezel, "Sensitivity and reliability of cerebral oxygenation responses to postural changes measured with near-infrared spectroscopy," *Eur. J. Appl. Physiol.*, vol. 119, no. 5, pp. 1117–1125, May 2019.

[30] K. Yoshitani et al., "Effects of hemoglobin concentration, skull thickness, and the area of the cerebrospinal fluid layer on near-infrared spectroscopy measurements," *Anesthesiology*, vol. 106, no. 3, pp. 458–462, Mar. 2007.

[31] J. M. Murkin and M. Arango, "Near-infrared spectroscopy as an index of brain and tissue oxygenation," *Brit. J. Anaesthesia*, vol. 103, pp. 3–13, Dec. 2009.

[32] A. M. Rahmani et al., "Artificial intelligence approaches and mechanisms for big data analytics: A systematic study," *PeerJ Comput. Sci.*, vol. 7, p. e488, Apr. 2021.

[33] C. Fraley and A. E. Raftery, "Model-based clustering, discriminant analysis, and density estimation," *J. Amer. Stat. Assoc.*, vol. 97, no. 458, pp. 611–631, Jun. 2002.

[34] J. Jacques and C. Preda, "Functional data clustering: A survey," *Adv. Data Anal. Classification*, vol. 8, no. 3, pp. 231–255, Sep. 2014.

[35] K. Cao et al., "Identifying and validating subtypes of Parkinson's disease based on multimodal MRI data via hierarchical clustering analysis," *Frontiers Hum. Neurosci.*, vol. 16, Jul. 2022, Art. no. 919081.

[36] S. B. Rosenthal et al., "Mapping the common gene networks that underlie related diseases," *Nature Protocols*, vol. 18, no. 6, pp. 1745–1759, Jun. 2023.

[37] J. E. McDermott et al., "Challenges in biomarker discovery: Combining expert insights with statistical analysis of complex omics data," *Exp. Opinion Med. Diag.*, vol. 7, no. 1, pp. 37–51, Jan. 2013.

[38] (Mar. 29, 2024). *Where Are We Now?* [Online]. Available: https://tilda.tcd.ie/about/where-are-we-now/

[39] S. P. Knight, L. Newman, J. D. O'Connor, J. Davis, R. A. Kenny, and R. Romero-Ortuno, "Associations between neurocardiovascular signal entropy and physical frailty," *Entropy*, vol. 23, no. 1, p. 4, Dec. 2020.

[40] I. Guelen et al., "Finometer, finger pressure measurements with the possibility to reconstruct brachial pressure," *Blood Pressure Monitor.*, vol. 8, no. 1, pp. 27–30, Feb. 2003.

[41] J. Cho, "Current status and prospects of health-related sensing technology in wearable devices," *J. Healthcare Eng.*, vol. 2019, pp. 1–8, Jun. 2019.

[42] G. Parati, R. Casadei, A. Groppelli, M. Di Rienzo, and G. Mancia, "Comparison of finger and intra-arterial blood pressure monitoring at rest and during laboratory testing," *Hypertension*, vol. 13, pp. 647–655, Jun. 1989.

[43] A. E. Schutte, H. W. Huisman, J. M. van Rooyen, N. T. Malan, and R. Schutte, "Validation of the finometer device for measurement of blood pressure in black women," *J. Hum. Hypertension*, vol. 18, no. 2, pp. 79–84, Feb. 2004.

[44] F. Scholkmann et al., "A review on continuous wave functional near-infrared spectroscopy and imaging instrumentation and methodology," *NeuroImage*, vol. 85, pp. 6–27, Jan. 2014.

[45] L. Cortese et al., "Performance assessment of a commercial continuous-wave near-infrared spectroscopy tissue oximeter for suitability for use in an international, multi-center clinical trial," *Sensors*, vol. 21, no. 21, p. 6957, Oct. 2021.

[46] T. Pham, K. Tgavalekos, A. Sassaroli, G. Blaney, and S. Fantini, "Quantitative measurements of cerebral blood flow with near-infrared spectroscopy," *Biomed. Opt. Exp.*, vol. 10, no. 4, pp. 2117–2134, 2019.

[47] M. Ferrari, M. Muthalib, and V. Quaresima, "The use of near-infrared spectroscopy in understanding skeletal muscle physiology: Recent developments," *Phil. Trans. Roy. Soc. A, Math., Phys. Eng. Sci.*, vol. 369, no. 1955, pp. 4577–4590, Nov. 2011.

[48] D. A. Boas, C. E. Elwell, M. Ferrari, and G. Taga, "Twenty years of functional near-infrared spectroscopy: Introduction for the special issue," *NeuroImage*, vol. 85, pp. 1–5, Jan. 2014.

[49] L. Newman, H. Nolan, D. Carey, R. B. Reilly, and R. A. Kenny, "Age and sex differences in frontal lobe cerebral oxygenation in older adults—Normative values using novel, scalable technology: Findings from the Irish longitudinal study on ageing (TILDA)," *Arch. Gerontol. Geriatrics*, vol. 87, Mar. 2020, Art. no. 103988.

[50] G. H. Klem, H. O. Luders, H. H. Jasper, and C. Elger, "The ten-twenty electrode system of the international federation. The international federation of clinical neurophysiology," *Electroencephalogr. Clin. Neurophysiol.*, vol. 52, pp. 3–6, Jan. 1999.

[51] F. Xue et al., "Were frailty identification criteria created equal? A comparative case study on continuous non-invasively collected neurocardiovascular signals during an active standing test in the Irish longitudinal study on ageing (TILDA)," *Sensors*, vol. 24, no. 2, p. 442, Jan. 2024.

[52] J. D. O'Connor, M. D. L. O'Connell, H. Nolan, L. Newman, S. P. Knight, and R. A. Kenny, "Impact of standing speed on the peripheral and central hemodynamic response to orthostasis: Evidence from the Irish longitudinal study on ageing," *Hypertension*, vol. 75, no. 2, pp. 524–531, Feb. 2020.

[53] E. Duggan, S. P. Knight, and R. Romero-Ortuno, "Relationship between sarcopenia and orthostatic blood pressure recovery in older falls clinic attendees," *Eur. Geriatric Med.*, vol. 14, no. 3, pp. 439–446, Apr. 2023.

[54] J. Paparrizos and L. Gravano, "K-shape: Efficient and accurate clustering of time series," *ACM SIGMOD Rec.*, vol. 45, no. 1, pp. 69–76, Jun. 2016.

[55] R. Tibshirani, G. Walther, and T. Hastie, "Estimating the number of clusters in a data set via the gap statistic," *J. Roy. Stat. Soc., B, Stat. Methodol.*, vol. 63, no. 2, pp. 411–423, May 2001.

[56] F. Xue, S. P. Knight, E. Connolly, E. Duggan, and R. Romero-Ortuno, "Functional clustering of continuous cardiovascular and brain oxygenation signals during an active stand test in the Irish longitudinal study on ageing (TILDA)," in *Proc. 31st Eur. Signal Process. Conf. (EUSIPCO)*, Sep. 2023, pp. 1080–1084.

[57] M. C. R. Briggs et al. (2017). *Health and Wellbeing: Active Ageing for Older Adults in Ireland—Evidence From The Irish Longitudinal Study on Ageing*. [Online]. Available: https://www.tilda.ie

[58] A. Sardá-Espinosa, "Time-series clustering in R using the dtwclust package," *R J.*, vol. 11, no. 1, pp. 22–43, 2019.

[59] J. S. Andrews, U. Desai, N. Y. Kirson, M. L. Zichlin, D. E. Ball, and B. R. Matthews, "Disease severity and minimal clinically important differences in clinical outcome assessments for Alzheimer's disease clinical trials," *Alzheimer's Dementia, Transl. Res. Clin. Interventions*, vol. 5, no. 1, pp. 354–363, Jan. 2019.

[60] L. K. Fitzgibbon-Collins, G. A. Heckman, I. Bains, M. Noguchi, W. E. McIlroy, and R. L. Hughson, "Older adults' drop in cerebral oxygenation on standing correlates with postural instability and may improve with sitting prior to standing," *Journals Gerontol., Ser. A*, vol. 76, no. 6, pp. 1124–1133, May 2021.

[61] M. Klop et al., "Capturing postural blood pressure dynamics with near-infrared spectroscopy-measured cerebral oxygenation," *GeroScience*, vol. 45, no. 4, pp. 2643–2657, Apr. 2023.

[62] L. Pérez-Denia, P. Claffey, L. Byrne, C. Rice, R. A. Kenny, and C. Finucane, "Increased multimorbidity is associated with impaired cerebral and peripheral hemodynamic stabilization during active standing," *J. Amer. Geriatrics Soc.*, vol. 70, no. 7, pp. 1973–1986, Jul. 2022.

[63] M. Ward et al., "Linking death registration and survey data: Procedures and cohort profile for the Irish longitudinal study on ageing (TILDA)," *HRB Open Res.*, vol. 3, p. 43, Nov. 2020.

Feng Xue received the Bachelors of Engineering degree (Hons.) mechanical engineering from Dublin Institute of Technology, Dublin, Ireland, in 2006, and the M.Sc. and Ph.D. degrees in bioengineering from Trinity College Dublin, Dublin, in 2008 and 2013, respectively.

He is a Research Fellow with Trinity College Dublin. His current research focus is in the area of signal processing and data analytics in biomedical engineering.

Silvin Knight, photograph and biography not available at the time of publication.

Emma Connolly, photograph and biography not available at the time of publication.

Morgana Afonso Shirsath, photograph and biography not available at the time of publication.

Louise Newman, photograph and biography not available at the time of publication.

Eoin Duggan, photograph and biography not available at the time of publication.

Rose Anne Kenny, photograph and biography not available at the time of publication.

Roman Romero-Ortuno, photograph and biography not available at the time of publication.